

Article

UV-Catalyzed Persulfate Oxidation of an Anthraquinone Based Dye

Kamil Krawczyk ^{1,*}, Stanisław Waclawek ^{1,*}, Edyta Kudlek ², Daniele Silvestri ^{1,*},
Tomasz Kukulski ³, Klaudiusz Grubel ⁴, Vinod V. T. Padil ¹ and Miroslav Černík ¹

¹ Institute for Nanomaterials, Advanced Technologies and Innovation, Technical University of Liberec, Studentská 1402/2, 46117 Liberec 1, Czech Republic; kamil.krawczyk@tul.cz (K.K.); vinod.padil@tul.cz (V.V.T.P.); miroslav.cernik@tul.cz (M.Č.)

² Department of Water and Wastewater Engineering, Silesian University of Technology, Konarskiego 18, 44-100 Gliwice, Poland; edyta.kudlek@polsl.pl

³ Institute of Textile Engineering and Polymer Materials, University of Bielsko-Biala, Willowa 2, 43-309 Bielsko-Biala, Poland; tkukulski@ath.bielsko.pl

⁴ Institute of Environmental Protection and Engineering, University of Bielsko-Biala, Willowa 2, 43-309 Bielsko-Biala, Poland; kgrubel@ath.bielsko.pl

* Correspondence: stanislav.waclawek@tul.cz (S.W.); daniele.silvestri@tul.cz (D.S.)

Received: 15 March 2020; Accepted: 21 April 2020; Published: 23 April 2020



Abstract: Wastewater from the textile industry has a substantial impact on water quality. Synthetic dyes used in the textile production process are often discharged into water bodies as residues. Highly colored wastewater causes various of problems for the aquatic environment such as: reducing light penetration, inhibiting photosynthesis and being toxic to certain organisms. Since most dyes are resistant to biodegradation and are not completely removed by conventional methods (adsorption, coagulation-flocculation, activated sludge, membrane filtration) they persist in the environment. Advanced oxidation processes (AOPs) based on hydrogen peroxide (H₂O₂) have been proven to decolorize only some of the dyes from wastewater by photocatalysis. In this article, we compared two very different photocatalytic systems (UV/peroxydisulfate and UV/H₂O₂). Photocatalyzed activation of peroxydisulfate (PDS) generated sulfate radicals (SO₄^{•−}), which reacted with the selected anthraquinone dye of concern, Acid Blue 129 (AB129). Various conditions, such as pH and concentration of PDS were applied, in order to obtain an effective decolorization effect, which was significantly better than in the case of hydroxyl radicals. The kinetics of the reaction followed a pseudo-first order model. The main reaction pathway was also proposed based on quantum chemical analysis. Moreover, the toxicity of the solution after treatment was evaluated using *Daphnia magna* and *Lemna minor*, and was found to be significantly lower compared to the toxicity of the initial dye.

Keywords: photocatalysis; dye; UV; peroxydisulfate; advanced oxidation process

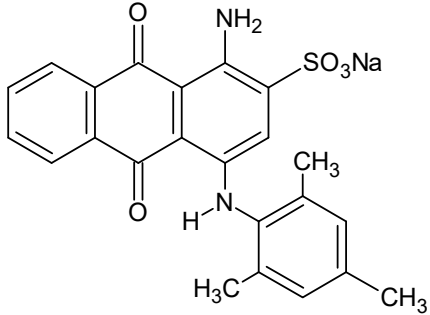
1. Introduction

A source of clean water is important for various industrial, social and economic development sectors; therefore, it has to be constantly monitored for impurities. Increased human activity has introduced a wide range of toxic chemicals including inorganic (e.g., chromium, mercury, lead) and organic (e.g., pesticides, surfactants, pharmaceuticals) pollutants into the aqueous environment [1,2]. A significant source of such polluting compounds is wastewater from the textile industry, which is classified as the most polluting of all industrial sectors in terms of effluent volume and its chemical content [3]. The chemical loads of textile effluents originate from the residues of textile production

processes, such as printing, scouring, bleaching and dyeing [4]. During the batch dyeing process, which is a common method for dyeing textiles, approximately 10% to 15% of the synthetic dyes used are lost, due to the inefficiency of the operation [5]. The residues are discharged into the effluent, from which they cannot be effectively removed by conventional wastewater treatment processes [6].

Dyes may be classified by their application or chemical structure into direct dyes (polyazo compounds, stilbenes, oxazines), basic dyes (diazahemicyanine, hemicyanine, cyanine, thiazine, acridine) or solvent dyes (azo, anthraquinone) [7]. Polyazo dyes have three or more N=N bonds in the molecule, and the number of azo groups attached to its center determines the color index of the dye (CI, systematic classification of colors by their saturation, brightness and hue) [8]. Designed to be highly stable towards light, temperature, water and detergents, dyes persist in the environment [9]. The presence of one or more benzene rings in their structure makes them more recalcitrant to biodegradation [10]. Moreover, dyes discharged into water even at a low concentration (even below 1 mg/L) are not only highly visible, which affects the aesthetic quality and transparency of water bodies (lakes, rivers) [11], but they also disturb the aquatic life by reducing light penetration and inhibiting photosynthesis, which causes oxygen deficiency [12]. Azo and anthraquinone dyes represent around 90% of all organic colorants [13]. They pose a threat to aquatic organisms (bacteria, algae, fish) by being toxic (lethal effect, genotoxic, mutagenic, carcinogenic) [14,15]. In particular, Acid Blue 129 (AB129), which is an acidic dye with an anthraquinone structure, being extensively used in the dyeing of silk, wool, cotton, paper, leather and nylon [16], was found to be associated with an ecotoxic hazard and danger of bioaccumulation [17]. The properties and structure of Acid blue 129 (AB129) are described in Table 1.

Table 1. Acid blue 129 (AB129) properties and structure

Chemical Formula: $C_{23}H_{19}N_2NaO_5S$	
Name: Sodium-1-amino-4-(2, 4, 6-trimethylanilino) anthraquinone-2-sulfonate	
Molecular weight: 458.46	
{Melting point: >300 °C	

Acid blue 129 structure

The conventional treatments of textile effluents involve, among others things: adsorption, coagulation-flocculation, membrane filtration and activated sludge [18,19]. However, these methods are not completely efficient and have several shortcomings. The adsorption process usually involves the use of activated carbon, which is expensive and incurs additional to regeneration and disposal costs [20]. Several dyes can inhibit bacteria development in activated sludge or cause membrane fouling using the filtration method [21,22]. Coagulation–flocculation is a pH-dependent process, which generates an extensive amount of concentrated sludge and is not suitable for all dyes [23].

Considering the obstacles in conventional textile wastewater treatment, alternative methods were developed. One of which is the advanced oxidation process (AOP), which utilizes highly reactive oxidizing intermediates like hydroxyl radicals ($\bullet OH$) [24]. These radicals are often catalytically generated from hydrogen peroxide (H_2O_2) or ozone. For example, the Fenton reaction uses iron as a catalyst for producing $\bullet OH$. AOPs can also utilize ozone (O_3) to produce $\bullet OH$, which is used for decolorization of the azo dyes C.I. Reactive black 5 [25]. Ultraviolet (UV) radiation can catalyze the generation of $\bullet OH$ by photolysis of H_2O_2 . This process was reported to be effective in the degradation of some dyes [26,27]. UV is also extensively used in combination with O_3 [28]. In one study, besides acting as a catalyst, UV radiation also contributed to the enhanced removal of total organic carbon (TOC) and

chemical oxygen demand (COD), in a decolorization experiment of Reactive Blue 19 [29]. While the oxidation-reduction potential (ORP) of $\bullet\text{OH}/\text{H}_2\text{O}$ is 2.8 V (at an acidic pH) and $\bullet\text{OH}/\text{OH}^-$ is 1.89 V (at an alkaline pH) [30], the use of H_2O_2 to generate radicals is not cost-effective. For example, Argun and Karatas [31] reported that 4 g/L of H_2O_2 and 0.2 g/L of iron salt were used to decolorize 200 mg/L of synthetic dye. Similarly, Meric et al. [32] used 0.4 g/L of H_2O_2 and 0.1 g/L of iron salt to decolorize 100 mg/L of dye. Therefore, high consumption of H_2O_2 provides an economical challenge and increases the need to find cheaper and more effective substitutes, e.g., permanganate, ozone, persulfate anions or sulfate radicals [33]. Sulfate radicals ($\text{SO}_4^{\bullet-}$) and $\bullet\text{OH}$ -based oxidation processes have comparable reaction rates for the removal of some pharmaceuticals [34], but sulfate radicals usually have a longer half-life (30–40 μs) than $\bullet\text{OH}$ (10^{-3} μs) [35,36]. Both radicals differ also in their reaction behavior, whereby $\text{SO}_4^{\bullet-}$ favors electron transfer and $\bullet\text{OH}$ reacts more by addition and H-abstraction [37,38]. This is reflected in the different types of dyes treated. For example, Tang and Huren [39] reported that $\bullet\text{OH}$ is ineffective for the oxidation of anthraquinone dyes, while degradation by $\text{SO}_4^{\bullet-}$ is effective [40]. $\text{SO}_4^{\bullet-}$ may be generated by catalytic activation of peroxydisulfate (PDS) by: heat, UV radiation, transition metals, electrolysis, transition metals or radiolysis [41,42]. While PDS in the form of sodium persulfate is cheaper (0.74 USD/kg) [43] and safer to handle than liquid H_2O_2 (1.5 USD/kg), it is more expensive if calculated per mol (0.18 USD/mol PDS, 0.05 USD/mol H_2O_2), and hence the amount of radicals generated. Despite the many advantages of persulfate treatment, its disadvantages also have to be taken into consideration, such as post-treatment toxicity. Post-contamination with sulfate salts may be thought a small problem in comparison to the toxic by-products formed in a $\text{SO}_4^{\bullet-}$ system, including transformation products of target contaminants (e.g., polynitrophenol compounds formed from nitrophenols [44]) and the by-products generated from effluent organic matter. $\text{SO}_4^{\bullet-}$ is known to be more prone to form such post-contamination; therefore, toxicity studies after persulfate treatment are recommended [41].

In this study, photocatalyzed decolorization experiments of anthraquinone dye AB129 were conducted under various conditions. The work was performed to evaluate the role of sulfate and hydroxyl radicals in the dye oxidation. Pseudo-first order rate kinetics were also evaluated, and a simple pathway was proposed. Finally, the post-treatment toxicity of by-products was measured. To the best of our knowledge, this is the first time that the UV application of PDS has been used for the catalyzed oxidation of anthraquinone dye. Table 2 shows the various methods used to degrade anthraquinone dyes.

Table 2. Methods used to degrade anthraquinone dyes.

Method Used	Dye	Decolorization [%]/Time [h]	Reference
AOP (wet air, wet peroxide, Fenton, photocatalytic,)	Reactive Blue 4	100%, 100%, 99%/1 and 100%/0.75	[45]
AOP (TiO_2 and ZnO nanoparticles + photodegradation)	Reactive Blue 19	>95%/0.5	[46]
AOP (ozonation)	Reactive Blue 19	~100%/0.3	[47]
AOP (TiO_2 + photodegradation)	Reactive Blue 19	~75%/3	[48]
AOP (Fenton reaction with pyrite ash)	Reactive Blue 4	100%/0.5	[49]
UV radiation and ozonation	Reactive Blue 19	100%/0.1	[50]
AOP (Fenton, photo-Fenton), UV radiation	Reactive Blue 19	81%, 98%, 42%/0.3	[51]
AOP (Sulfate radical + UV)	Acid Blue 129	87%/1	This work

2. Results and Discussion

Several experiments were performed, including the influence of $\bullet\text{OH}$ and $\text{SO}_4^{\bullet-}$ on the decolorization efficiency, effect of PDS concentration, pH, possible reaction pathways, and the ecotoxicity of by-products.

2.1. Influence of $\bullet\text{OH}$ and $\text{SO}_4^{\bullet-}$ on AB129 Decolorization

To determine the decolorization efficiency of both radical species on AB129, we performed experiments with PDS (source of $\text{SO}_4^{\bullet-}$) and H_2O_2 ($\bullet\text{OH}$) catalyzed by UV. It is known that from 1 mole of oxidant, 2 moles of radicals may be generated, according to Equations (1) and (2):



Figure 1 shows that UV irradiation alone [similarly to PDS (Figure 2) and H_2O_2 (data not shown) w/o UV activation] was not able to degrade the dye. The dye seems to be resistant to direct UV photolysis, as the energy of the photons with a wavelength ranging from 313 to 578 nm is too low to degrade the molecule of the dye. Also, decolorization by $\bullet\text{OH}$ is relatively slow and reached only 12% after one hour of the experiment. Only the UV-catalyzed $\text{SO}_4^{\bullet-}$ oxidation process was found to be effective in the decolorization of AB129, whereby the effect was about 90% of the initial dye concentration (25 mg/L). Homolysis of the peroxide bond of PDS occurs when catalyzed by UV, which results in the generation of $\text{SO}_4^{\bullet-}$ [52]. In proposed UV/PDS system (in near neutral or acidic pH) the only type of free radicals formed could be $\text{SO}_4^{\bullet-}$. Water molecules could be oxidized to produce $\bullet\text{OH}$ but this process is very slow ($k = 6.6 \times 10^2 \text{ s}^{-1}$) [53] and therefore, not significant in the timeframe of the experiment.

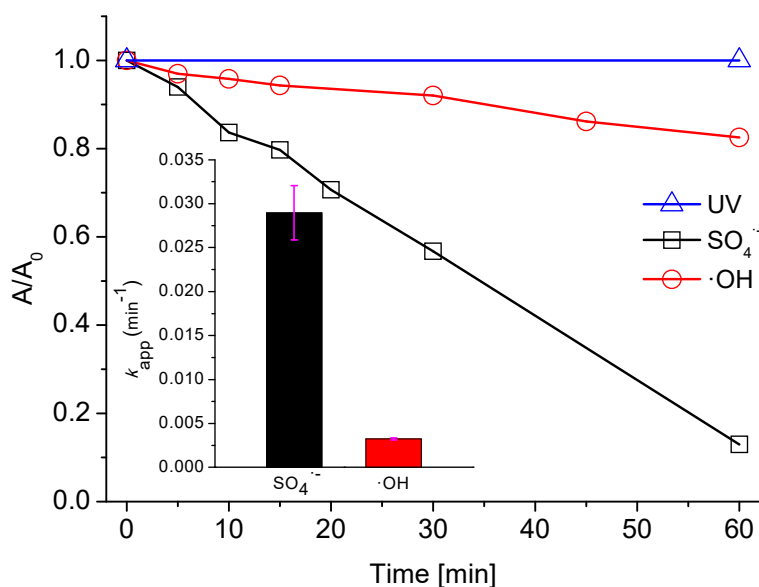


Figure 1. Decolorization (absorbance at 595 nm) of AB129 with $\text{SO}_4^{\bullet-}$, $\bullet\text{OH}$ and ultraviolet (UV) radiation alone (conditions: 25 mg/L AB129, 2.5 mM PDS, 10 mM H_2O_2 , UV 150 W). The inset shows decolorization kinetics of AB129 by $\text{SO}_4^{\bullet-}$ and $\bullet\text{OH}$, (the fuchsia error bars represent the slope error).

Despite the H_2O_2 concentrations being four times higher than in the case of PDS (10 mM vs. 2.5 mM), the generated $\bullet\text{OH}$ radicals did not react with the AB129 as effectively due to the following possible reasons. Although H_2O_2 and PDS molecules have a similar bond length of 1.453 Å and 1.497 Å [54], H_2O_2 peroxide bond energy (51.0 kcal/mol) is significantly higher than PDS (33.5 kcal/mol) and, therefore, it is more difficult to be cleaved by UV irradiation [55]. Furthermore, $\bullet\text{OH}$ has an almost ten times faster recombination rate ($k = 5.2 \times 10^9 \text{ M}^{-1} \text{ s}^{-1}$) [56] than $\text{SO}_4^{\bullet-}$ ($k = 5.0 \times 10^8 \text{ M}^{-1} \text{ s}^{-1}$) [57] and, therefore, a smaller amount of generated radicals is available to react with the contaminant, compared to $\text{SO}_4^{\bullet-}$. Further differences in the decolorization of AB129 may be due to intrinsic differences in the reaction mechanisms. While $\text{SO}_4^{\bullet-}$ works more by electron abstraction because of a

higher electron affinity (2.43 eV) than $\bullet\text{OH}$ (1.83 eV), $\bullet\text{OH}$ acts more through hydrogen abstraction or addition [58]. This makes $\text{SO}_4^{\bullet-}$ more selective and highly reactive towards organic contaminants containing non-bonding electron pairs of atoms such as O, N and S [59]. The first steps of the reaction between AB129 and sulfate radicals are described in more detail in the subsection “Formation of by-products”.

The apparent first order (k_{app}) rate constants, shown in the inset of Figure 1 and calculated based on Equation (9), are one order of magnitude different higher for $\text{SO}_4^{\bullet-}$ than for $\bullet\text{OH}$ (0.029 min^{-1} and 0.0032 min^{-1} for $\text{SO}_4^{\bullet-}$ and $\bullet\text{OH}$, respectively). Both radicals are susceptible to electron transfer; however, $\text{SO}_4^{\bullet-}$ shows a much lower energy barrier for this reaction, which results in markedly higher k_{app} . Therefore, it was decided to focus solely on PDS for a better understanding of its reaction mechanism with the AB129 dye.

2.2. Effect of PDS Concentration

To determine the optimal decolorization conditions, the concentration of PDS was changed from 0.625 to 2.5 mM, as depicted in Figure 2, where the inset shows the decolorization kinetics of AB129 by different PDS concentrations.

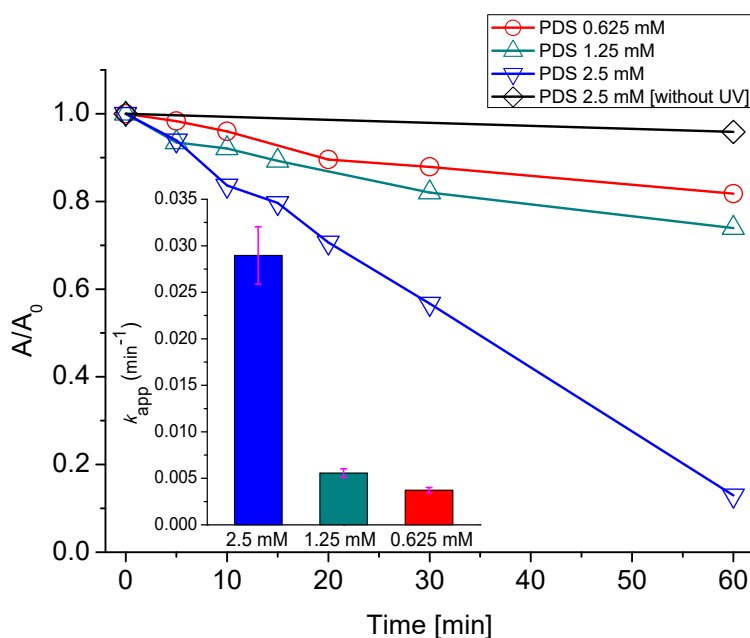


Figure 2. Decolorization (absorbance at 595 nm) of AB129 by UV/peroxydisulfate (PDS) system (25 mg/L AB129, UV 150 W). The fuchsia error bars represent the slope error

The concentrations of 0.625 mM and 1.25 mM achieved only 18% and 26% decolorization, respectively, and are almost comparable with the blank experiment w/o UV light. A further increase to 2.5 mM caused a significant improvement. The kinetic of the dye removal is significantly faster, the decrease is linear, and after 60 min the dye decolorization reached 87%. The apparent first-order rate constants calculated were 0.0037 min^{-1} , 0.0056 min^{-1} and 0.029 min^{-1} for 0.625 mM, 1.25 mM and 2.5 mM PDS, respectively. Therefore, for the four-fold increase in the PDS concentration, the rate constant increased roughly eight times. This may be because the low concentrations of oxidant did not produce enough $\text{SO}_4^{\bullet-}$ to degrade the dye effectively [60]. Finally, 2.5 mM was chosen as the optimal concentration in the experiment in terms of efficiency and economy, because higher PDS concentrations are not economically feasible.

2.3. Effect of the Initial pH

The other parameter that significantly influences the decolorization efficiency is the initial pH of the solution. The initial solution pH was varied in the interval between 3 and 11, as shown in Figure 3.

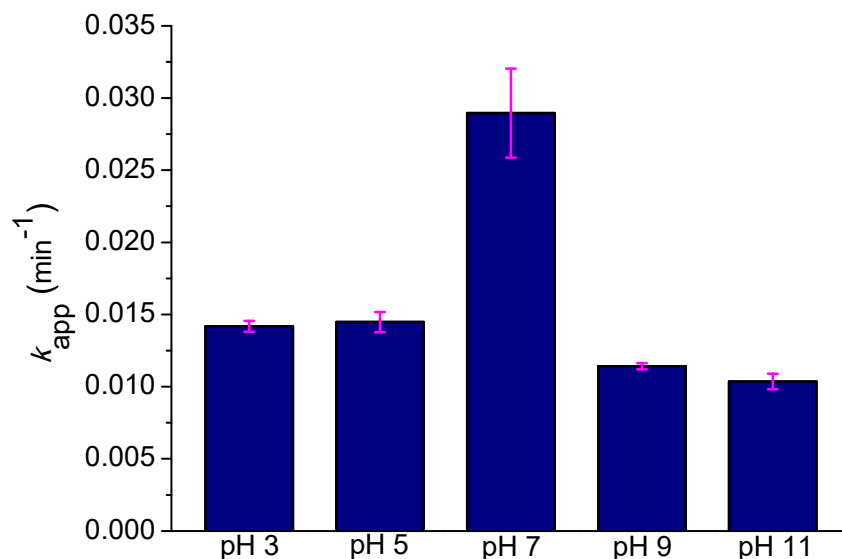
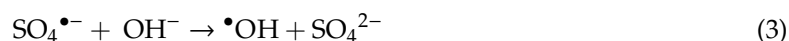


Figure 3. Effect of the initial pH on AB129 decolorization rate constant (conditions: 25 mg/L AB129, absorbance measured at 595 nm, UV 150 W). The fuchsia error bars represent the slope error.

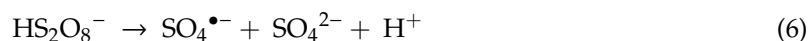
It can be inferred that the pH conditions had a significant influence on the UV catalyzed PDS oxidation system. The apparent first-order rate constant increased noticeably from the pH range of 3 to 5 (0.0141 min^{-1} and 0.0145 min^{-1}) to pH 7 (0.029 min^{-1}) and decreased back to half-values for a higher pH (0.0114 min^{-1} and 0.0107 min^{-1} for pH 9 and 11, respectively). The results show that the neutral conditions are the most optimal for the decolorization reaction. Under an alkaline pH, the hydroxides (OH^-) in the solution undergo reactions with $\text{SO}_4^{\bullet-}$ to generate $\bullet\text{OH}$ (Equation (3)), which is a significantly less effective radical species in this respect.



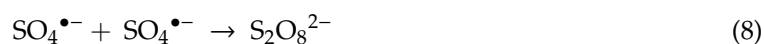
Furthermore, the generated $\bullet\text{OH}$ further reacts with $\text{SO}_4^{\bullet-}$ (Equation (4)), decreasing the number of available radicals.



Under an acidic pH, the further breakdown of PDS to $\text{SO}_4^{\bullet-}$ may be catalyzed by acid activation (Equation (5) and (6)).



However, the generation of $\text{SO}_4^{\bullet-}$ catalyzed by acid conditions and UV together would yield high concentrations of those radicals. In excess, $\text{SO}_4^{\bullet-}$ may favor reactions like scavenging (Equation (7)) [61] or recombination (Equation (8)) over reactions with the dye.



This may explain k_{app} being lower in an acidic pH compared to a neutral pH, which was also observed by Liang et al. [62] in a PDS oxidation system. Overall, the most favorable condition for

oxidation of AB129 is at pH of 7. Alkaline and acidic pH conditions caused inhibition of the reaction by the possible reasons explained. After evaluating the effect of pH on the decolorization process, the study focused on the identification of post-treatment intermediates.

2.4. Formation of by-Products

To determine the possible formation of by-products, the absorbance spectra during the decolorization of AB129 were recorded, as depicted in Figure 4.

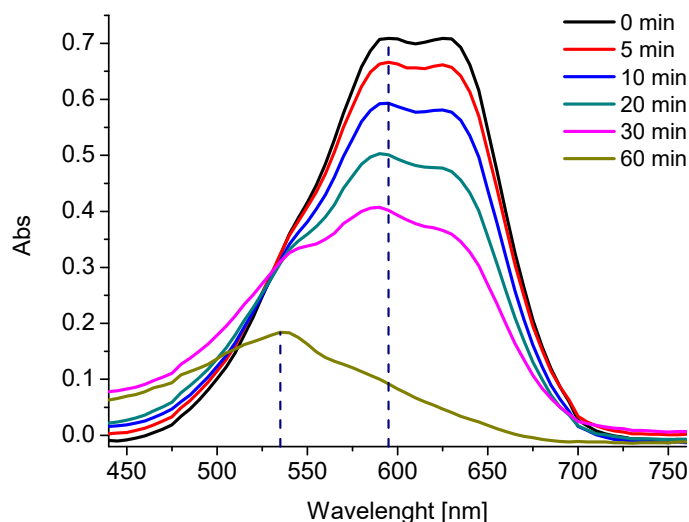


Figure 4. Absorbance spectra of AB129 during decolorization tests (conditions: 25 mg/L AB129, 2.5 mM PDS).

At the beginning, a double peak at 595 and 630 nm was recorded. During the experiment, the peak at 630 nm slowly disappeared, followed by the peak at 595 nm. At 20 min, a new peak at 535 nm was formed, which dominated at the end of the experiment (60 min). This peak may represent the formed by-products.

Quantum chemical calculations were performed to determine the most probable pathway of the reaction between the sulfate radical and AB129. Firstly, the geometry of AB129 was optimized, as shown in Figure 5.

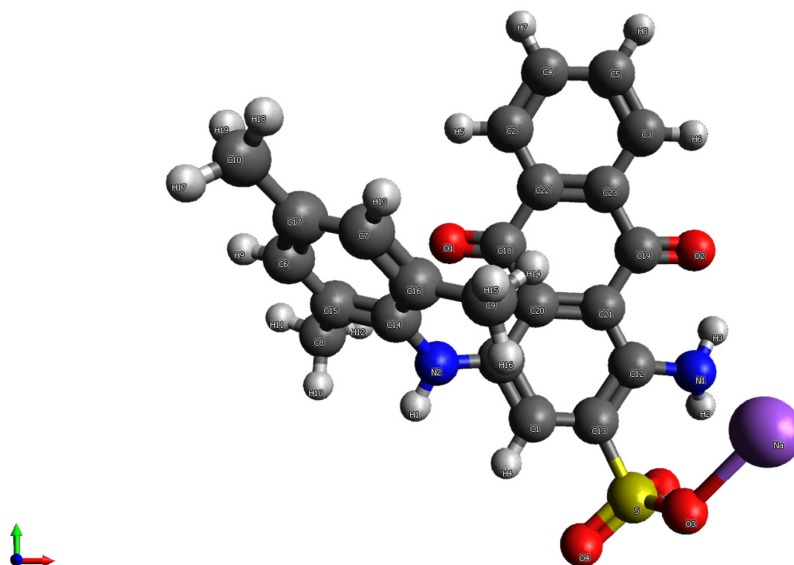


Figure 5. Optimized AB129 molecule obtained using B3LYP/6-31G**.

Then the CPCM approach was applied in order to model the solvent (water) effect on the calculated transition energies of the species with the def2-TZVP basis set. The λ_{\max} of the visible spectrum was computed to be 594 nm, almost the same as the wavelength, which was used for determination of AB129 (595 nm), and corresponded to the HOMO \rightarrow LUMO and HOMO-1 \rightarrow LUMO (overall $E = 2.087$ eV) transitions of AB129. Moreover, the values of HOMO and LUMO were found to be -5.413 and -2.863 eV, respectively, whereas the difference in the energy (HOMO-LUMO energy gap) was 2.55 eV. Similar values were recently computed and reported for Acid Blue 113 by Asghar et al. [63]. Figure 6 shows the HOMO and LUMO of AB129 obtained at B3LYP/6-31G** and a map of the electron density of the AB129 molecule.

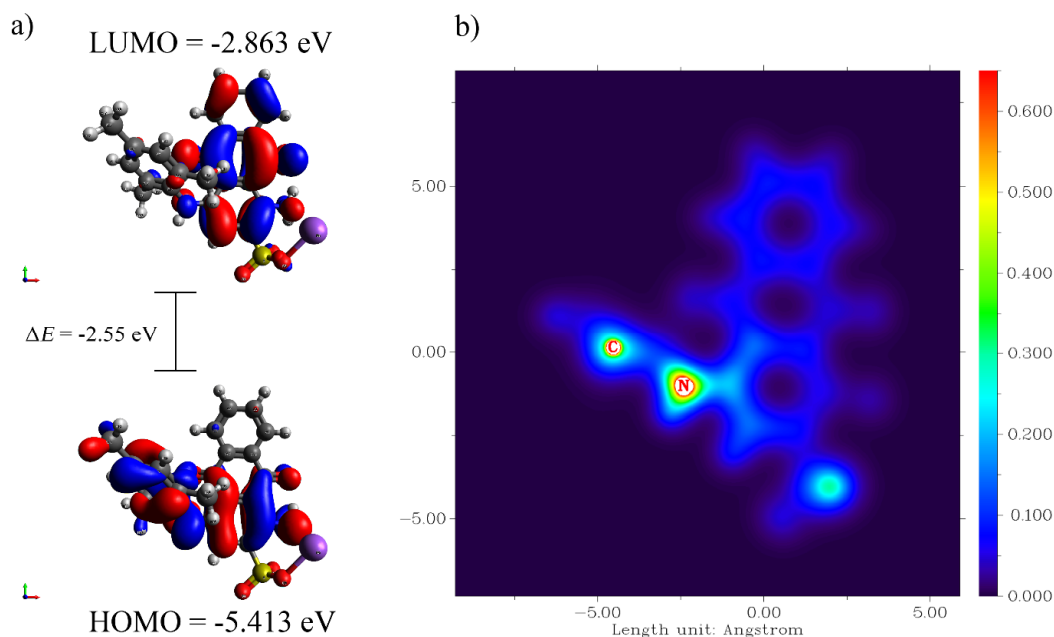


Figure 6. (a) HOMO and LUMO of AB129 obtained at B3LYP/6-31G** and (b) map of the electron density (X, Y plane) of AB129 molecule (the sodium atom was removed for simplicity).

According to the frontier orbital theory, chemical reactions preferentially occur at the position of the molecule wherein their frontier orbital intensely overlap [64]. Moreover, the most probable reaction pathway for sulfate radicals that have a very strong electrophilic character is a direct attack on one of the atoms of the contaminant molecule, usually the one with the highest electron density in the HOMO of the aromatic molecule [65]. Figure 6b shows that one of the positions with the highest electron densities (in the HOMO of AB129) is the region near to nitrogen atom from the secondary amine. From this, it is possible to conclude that there is a higher preference for the $-\text{NH}-$ group, and that the main product forming in this system is a derivative of hydroxylated anthraquinone.

Furthermore, according to Liu et al. [66], a Hirshfeld charge may be successfully employed to determine the reactive sites of the electrophilic reactions. Apart from the oxygen atoms, which are probably not involved in the reactions reported in this study, and a high O/C ratio is often correlated with a slow reaction between the molecules and the oxidants [67], the N atom of AB129 may be characterized by the smallest Hirshfeld charge (-0.424), which is even smaller than the second nitrogen (N1: -0.398) from the primary amine located on the anthraquinone. This may provide further confirmation that the first and crucial reaction of the sulfate radical with AB129 is an electron transfer from the $-\text{NH}-$ moiety, which splits the AB129 molecule and creates the anthraquinone derivative.

This conclusion may be supported in several other ways. Primarily, the intermediate that was formed absorbs photons of higher energy (Vis peak shifted to the left side of the spectrum i.e., 535 nm), which is typical for the anthraquinone derivatives with a much lower molecular weight [39]. A similar

observation was made by Tang and An, who observed radical driven splitting of Acid Blue 40 with the formation of a yellow intermediate absorbing light in a similar region to that reported in this study [39].

Considering the possible formation of by-products, their toxicity on model plant fronds and freshwater crustaceans was evaluated and is discussed below.

2.5. Ecotoxicity

In addition to a determination of decolorization efficiency, it is important to consider the toxicity of the system for living organisms, since post-treatment by-products may sometimes be more toxic than the initial contaminant [41]. Tests using plant fronds *Daphnia magna* and freshwater crustaceans *Lemna minor* are often performed in toxicological studies, because they are simple, fast and cost-effective. Moreover, they represent both plants and animals, which may tell us more about the impact on the ecosystem, and selected microorganisms are very informative in terms of the potential toxicity of wastewater [68–70]. For example, Sackey et al. found that *Daphnia magna* and *Lemna minor* are effective for testing the toxicity of leachates [71]. Moreover, Castro et al. [72] investigated the potential toxicity of effluents from the textile industry before and after treatment, and concluded that the raw textile effluent was very toxic. Therefore, toxicity tests were performed using the same conditions mentioned in the methodology of the decolorization test, except different concentrations of PDS and AB129 were used, as shown in Tables 3 and 4.

Table 3. Toxicity of AB129 by-products on *Daphnia magna* (* Time 0 min = samples without PDS addition).

Daphnia Magna						
PDS/AB129 [mM]	Time [min]					
	0 *	5	10	20	30	45
Toxicity Effect [%]						
0.2/0.2	25	40	35	30	25	20
0.5/0.5	30	40	45	40	30	20
1/1	40	55	65	50	35	25
2/2	50	60	65	55	40	30

Table 4. Toxicity of AB129 by-products on *Lemna minor* (* Time 0 min = samples without PDS addition).

Lemna Minor						
PDS/AB129 [mM]	Time [min]					
	0 *	5	10	20	30	45
Toxicity Effect [%]						
0.2/0.2	8	17	8	0	0	0
0.5/0.5	25	25	25	8	0	0
1/1	33	25	33	17	8	8
2/2	33	33	25	17	17	17

According the guidelines for the interpretation of the obtained toxicity results given by Kudlek [73], samples characterized by a toxic effect of <25% are nontoxic. Only the lowest concentration of PDS/AB129 (0.2/0.2 mM) was nontoxic for the *Lemna minor* test organisms, whereas *Daphnia magna* organisms were more sensitive to the action of PDS/AB129, and classified the post-processed samples subjected to both 0.2/0.2 mM and 0.5/0.5 mM as low toxic (a toxicity effect of between 25% and 50%). A toxicity effect higher than 50% classified the samples as being toxic. Such results were noted in the samples between 5 and 20 min of the experiment tested on *Daphnia magna*, where the concentration of PDS/AB129 was equal to 1/1 mM and 2/2 mM.

Nonetheless, both tests indicated that the toxicity of the initial solutions increased along with the PDS/AB129 concentration. In both tests, up to approximately 10 min of the experiment, the toxicity increased due to the effect of the addition of PDS. However, in both cases, after this time, a decreasing trend in toxicity was detected. After 45 min of the experiment, the toxicity for *Daphnia* roughly halved for all of the concentrations analyzed and for *Lemna* it decreased even more. This may indicate that by-products of AB129 after treatment are less toxic than the original dye. Moreover, PDS toxicity is only temporary, because it is quickly decomposed and exhibits lower toxicity to the analyzed organisms.

3. Materials and Methods

3.1. Chemicals

Sodium persulfate ($\text{Na}_2\text{S}_2\text{O}_8$, purity $\geq 98\%$), hydrogen peroxide (H_2O_2 , 30% w/w in water), sodium hydroxide (NaOH , 97% powder), sulfuric acid (H_2SO_4 , 95%–98%), and Acid blue (AB129, $\text{C}_{23}\text{H}_{19}\text{N}_2\text{NaO}_5\text{S}$, 25% dye content) were purchased from Sigma Aldrich (Prague, Czech Republic). Hydrochloric acid (HCl , $>35\%$) was purchased from Avantor Performance Materials Poland (Gliwice, Poland). Deionized water ($18.2 \text{ M}\Omega\cdot\text{cm}$) obtained from ELGA purelab flex system (ELGA, Veolia Water, Marlow, UK) was used in all of the experiments.

3.2. Analytical

A pH meter TMultiLine® Multi 3430 IDS from WTW (Weilheim, Germany) equipped with SenTix pH electrodes was used to measure the acidity of the reaction mixture. The visible spectrum of the samples was measured by a UV-Vis spectrophotometer DR 3900 from Hach (Vancouver, WA, USA) within the 440–760 nm wavelength range, recorded every 5 nm.

3.3. Decolorization Test

Decolorization experiments of AB129 were performed based on a modified method of Neamtu et al. [74]. Firstly, a solution of AB129 (25 mg/L) and PDS (various concentrations of 0.625 mM, 1.25 mM and 2.5 mM) or H_2O_2 (10 mM) was prepared in a 100 mL reactor. Then, pH conditions were adjusted by adding a minimal amount of concentrated NaOH or H_2SO_4 solution, and the prepared reactor was exposed to UV radiation under constant magnetic stirring. The UV light source was provided by a model TQ 150 medium-pressure mercury UV lamp (Heraeus, Hanau, Germany) placed in a quartz glass (DURAN 50) cooling jacket fed by recirculating tap water. This step maintained a constant temperature of the mixture of $21 \pm 1^\circ\text{C}$. According to the data provided by the manufacturer, the TQ 150 lamp operated in the cooling jacket emanates radiation with a wavelength λ_{exc} of 313, 365, 405, 436, 546, 578 nm, and radiation flux equal to 2.5, 5.8, 2.9, 3.6, 4.6, 4.2 W, respectively. The absorbance spectra were measured in 1 mL quartz cuvettes by a UV-Vis spectrometer at the wavelength of 595 nm according to Palencia et al. [75]. The analyses were performed several times and averages and standard deviations were calculated by Origin 9 software [OriginLab].

3.4. Kinetic Test and AB129 Structure Modelling

A pseudo-first order kinetic model was used to describe the decolorization of AB129 by $\text{SO}_4^{\bullet-}$ and $\bullet\text{OH}$ (Equation (9)) [76].

$$\ln\left(\frac{C_t}{C_0}\right) = \ln\left(\frac{A_t}{A_0}\right) = -k_{\text{app}}t \quad (9)$$

where C_0 and C_t are the initial ($t = 0$) and time-dependent concentrations (at time t), proportional to the measured absorbance A , respectively, and k_{app} is an apparent rate constant [77].

3.5. Quantum Chemical Analysis

The initial coordinates of the AB129 structure were obtained with the Avogadro program [78]. The structure of the AB129 was further optimized using the Orca program package [79], and the results were validated with Gaussian 16 software [63], both in the gaseous and liquid phase at the B3LYP/6-31G** level of study, as suggested in a recent work on the Acid blue 113 oxidation [63]. Time-dependent density functional theory TD-DFT was used to predict the excited state properties of AB129. The outputs were later visualized with the Avogadro program, whereas the electron densities and Hirshfeld charges were visualized and computed by Multiwfn software [80,81].

3.6. Ecotoxicity Test

Two different bio-tests were used to determine the toxicity of the post-treatment products: the *Lemna* sp. growth inhibition test (GIT) and the Daphtoxkit F bioassay. In the GIT, plant fronds of freshwater vascular plants *Lemna minor* from our own breeding were used. The test is based on calculating the number of plant fronds growing for 7 days in a tested and blank sample, prepared according to the OECD Guideline 221. The test was performed at a temperature of 25 ± 1 °C by a constant exposure to light with an illuminance of 6000 lux.

The Daphtoxkit F bioassay from Tigrat (Warszawa, Poland) uses freshwater crustaceans *Daphnia magna* to measure their immobility or mortality after 24 h exposure to tested post-process samples, in comparison to standard freshwater (ISO medium prepared according ISO 6341). The test was performed on 1-day-old test organisms, according to the OECD Guideline 202. NaOH (0.1 mol/L) and HCl (0.1 mol/L) solutions were used for pH corrections during the toxicity tests. The toxicity of both tests was calculated using the following equation 10 [73]:

$$E = \frac{(N_C - N_T)}{N_C} \cdot 100\% \quad (10)$$

where E is the toxicity effect (%), N_C is the number of living organisms (plant fronds or freshwater crustaceans) in the control sample, and N_T is the number of living organisms (plant fronds or freshwater crustaceans) in the test sample. Interpretation of the results obtained from both of the toxicity tests was performed based on the toxicity classification presented in Table 5, and according to guidelines proposed by Mahugo Santana et al. [82].

Table 5. Interpretation of the toxicity results.

Toxicity Effect E%	Toxicity Classification
<25	non-toxic
25–50	low toxic
50.01–75	toxic
>75	highly toxic

4. Conclusions

In this work, we focused on sulfate and hydroxyl radical-based oxidation processes catalyzed by UV for the treatment of the model dye Acid Blue 129. $\text{SO}_4^{\bullet-}$ at a concentration of 2.5 mM successfully decolorized 25 mg/L of the dye up to 87% within 60 min, whereas $\bullet\text{OH}$ at a concentration of 10 mM was significantly less effective. The pseudo-first-order kinetic rate constant of the optimal reaction conditions, including neutral pH, was found to be 0.029 min^{-1} . The probable reaction pathway of AB129 with $\text{SO}_4^{\bullet-}$ was determined using quantum chemical calculations, indicating electron transfer from the $-\text{NH}-$ moiety, which splits the AB129 molecule creating the anthraquinone derivative. Ecotoxicity tests of the by-products showed a lower toxicity than the toxicity of the initial dye and only a temporary effect of PDS.

Author Contributions: Conceptualization, S.W. and K.K.; methodology, K.K. and S.W.; software, S.W.; validation, S.W., E.K. and M.Č.; investigation, T.K. and K.K.; writing—original draft preparation, K.K. and E.K.; writing—review and editing, K.G., S.W., D.S., V.V.T.P., and M.Č.; supervision, S.W. and M.Č. All authors have read and agreed to the published version of the manuscript

Funding: This research was supported by the Ministry of Education, Youth and Sports in the Czech Republic under the “Inter Excellence – Action programme” within the framework of the project “Exploring the role of ferrates and modified nano zero-valent iron in the activation process of persulfates” (registration number LTAUSA18078) and the Research Infrastructures NanoEnvicZ (Project No. LM2018124). This work was also supported by the Ministry of Education, Youth and Sports of the Czech Republic and the European Union - European Structural and Investment Funds in the frames of Operational Programme Research, Development and Education - project Hybrid Materials for Hierarchical Structures (HyHi, Reg. No. CZ.02.1.01/0.0/0.0/16_019/0000843). Finally, the work was supported by the Ministry of Science and Higher Education Republic of Poland within statutory funds No. 08/040/BK_19/0119, and by the National Centre for Research and Development in Poland (POIR.04.01.02-00-0062/16).

Conflicts of Interest: The authors declare no conflict of interest.

References

- Pal, A.; He, Y.; Jekel, M.; Reinhard, M.; Gin, K.Y.H. Emerging contaminants of public health significance as water quality indicator compounds in the urban water cycle. *Environ. Int.* **2014**, *71*, 46–62. [CrossRef]
- Tsiampalis, A.; Frontistis, Z.; Binas, V.; Kiriakidis, G.; Mantzavinos, D. Degradation of sulfamethoxazole using iron-doped titania and simulated solar radiation. *Catalysts* **2019**, *9*, 612. [CrossRef]
- Şen, S.; Demirer, G.N. Anaerobic treatment of real textile wastewater with a fluidized bed reactor. *Water Res.* **2003**, *37*, 1868–1878. [CrossRef]
- Ozturk, E.; Yetis, U.; Dilek, F.B.; Demirer, G.N. A chemical substitution study for a wet processing textile mill in Turkey. *J. Clean. Prod.* **2009**, *17*, 239–247. [CrossRef]
- Inoue, M.; Okada, F.; Sakurai, A.; Sakakibara, M. A new development of dyestuffs degradation system using ultrasound. *Ultrason. Sonochem.* **2006**, *13*, 313–320. [CrossRef]
- Eren, Z. Ultrasound as a basic and auxiliary process for dye remediation: A review. *J. Environ. Manag.* **2012**, *104*, 127–141. [CrossRef]
- Julkapli, N.M.; Bagheri, S.; Hamid, S.B.A. Recent advances in heterogeneous photocatalytic decolorization of synthetic dyes. *Sci. World J.* **2014**, *2014*, 692307. [CrossRef]
- Ghaly, A.E.; Ananthashankar, R.; Alhattab, M.; Ramakrishnan, V.V. Production, Characterization and Treatment of Textile Effluents: A Critical Review. *J. Chem. Eng. Process. Technol.* **2014**, *5*, 1000182.
- Chequer, F.D.; de Oliveira, G.A.R.; Ferraz, E.R.A.; Carvalho, J.; Zanoni, M.B.; de Oliveir, D.P. Textile Dyes: Dyeing Process and Environmental Impact. *Eco-Friendly Text. Dye. Finish.* **2013**, *6*, 151–176.
- Wang, J.; Guo, B.; Zhang, X.; Zhang, Z.; Han, J.; Wu, J. Sonocatalytic degradation of methyl orange in the presence of TiO₂ catalysts and catalytic activity comparison of rutile and anatase. *Ultrason. Sonochem.* **2005**, *12*, 331–337. [CrossRef]
- Wijetunga, S.; Li, X.F.; Jian, C. Effect of organic load on decolourization of textile wastewater containing acid dyes in upflow anaerobic sludge blanket reactor. *J. Hazard. Mater.* **2010**, *177*, 792–798. [CrossRef]
- Entezari, M.H.; Al-Hoseini, Z.S.; Ashraf, N. Fast and efficient removal of Reactive Black 5 from aqueous solution by a combined method of ultrasound and sorption process. *Ultrason. Sonochem.* **2008**, *15*, 433–437. [CrossRef] [PubMed]
- Crini, G.; Badot, P.-M. *Sorption Processes and Pollution: Conventional and Non-Conventional Sorbents for Pollutant Removal from Wastewaters*; Presses universitaires de Franche-Comté: Besançon, France, 2010; ISBN 2848673044.
- Puvaneswari, N.; Muthukrishnan, J.; Gunasekaran, P. Toxicity assessment and microbial degradation of azo dyes. *Indian J. Exp. Biol.* **2006**, *44*, 618–626.
- Oh, S.W.; Kang, M.N.; Cho, C.W.; Lee, M.W. Detection of carcinogenic amines from dyestuffs or dyed substrates. *Dye. Pigment.* **1997**, *33*, 119–135. [CrossRef]
- Fat’hi, M.R.; Asfaram, A.; Hadipour, A.; Roosta, M. Kinetics and thermodynamic studies for removal of Acid Blue 129 from aqueous solution by almond shell. *J. Environ. Health Sci. Eng.* **2014**, *12*, 26. [CrossRef] [PubMed]
- Acid Blue 129. Available online: <http://datasheets.scbt.com/sc-214468.pdf> (accessed on 22 April 2020).
- Pala, A.; Tokat, E. Color removal from cotton textile industry wastewater in an activated sludge system with various additives. *Water Res.* **2002**, *36*, 2920–2925. [CrossRef]

19. Harrelkas, F.; Azizi, A.; Yaacoubi, A.; Benhammou, A.; Pons, M.N. Treatment of textile dye effluents using coagulation-flocculation coupled with membrane processes or adsorption on powdered activated carbon. *Desalination* **2009**, *235*, 330–339. [[CrossRef](#)]
20. Cooper, P. Removing colour from dyehouse waste waters—A critical review of technology available. *J. Soc. Dye. Colour.* **1993**, *109*, 97–100. [[CrossRef](#)]
21. Fane, A.G.; Fell, C.J.D. A review of fouling and fouling control in ultrafiltration. *Desalination* **1987**, *62*, 117–136. [[CrossRef](#)]
22. Georgiou, D.; Melidis, P.; Aivasidis, A. Use of a microbial sensor: Inhibition effect of azo-reactive dyes on activated sludge. *Bioprocess Biosyst. Eng.* **2002**, *25*, 79–83.
23. Katheresan, V.; Kansedo, J.; Lau, S.Y. Efficiency of various recent wastewater dye removal methods: A review. *J. Environ. Chem. Eng.* **2018**, *6*, 4676–4697. [[CrossRef](#)]
24. Li, Q.; Wang, L.; Fang, X.; Zhang, L.; Li, J.; Xie, H. Synergistic effect of photocatalytic degradation of hexabromocyclododecane in water by UV/TiO₂/persulfate. *Catalysts* **2019**, *9*, 189. [[CrossRef](#)]
25. Tehrani, A.R.; Mahmood, N.M.; Arami, M. Study of the efficiency of effective parameters on decolorization of CI. Reactive black 5 wastewater by ozonation. *J. Color Sci. Technol.* **2008**, *2*, 67–75.
26. Muruganandham, M.; Swaminathan, M. Photochemical oxidation of reactive azo dye with UV-H₂O₂ process. *Dye. Pigment.* **2004**, *62*, 269–275. [[CrossRef](#)]
27. Mohey El-Dein, A.; Libra, J.A.; Wiesmann, U. Mechanism and kinetic model for the decolorization of the azo dye Reactive Black 5 by hydrogen peroxide and UV radiation. *Chemosphere* **2003**, *52*, 1069–1077. [[CrossRef](#)]
28. Lovato, M.E.; Gilliard, M.B.; Cassano, A.E.; Martín, A.M. Kinetics of the degradation of n-butyl benzyl phthalate using O₃/UV, direct photolysis, direct ozonation and UV effects. *Environ. Sci. Pollut. Res.* **2015**, *22*, 909–917. [[CrossRef](#)]
29. Tehrani-Bagha, A.R.; Amini, F.L. Decolorization of a Reactive Dye by UV-Enhanced Ozonation. *Prog. Col. Color. Coat.* **2010**, *3*, 1–8.
30. Ghernaout, D. Advanced oxidation phenomena in electrocoagulation process: A myth or a reality? *Desalin. Water Treat.* **2013**, *51*, 7536–7554. [[CrossRef](#)]
31. Argun, M.E.; Karatas, M. Application of Fenton process for decolorization of reactive black 5 from synthetic wastewater: Kinetics and thermodynamics. *Environ. Prog. Sustain. Energy* **2011**, *30*, 540–548. [[CrossRef](#)]
32. Meriç, S.; Kaptan, D.; Ölmez, T. Color and COD removal from wastewater containing Reactive Black 5 using Fenton's oxidation process. *Chemosphere* **2004**, *54*, 435–441. [[CrossRef](#)]
33. Li, J.; Li, R.; Zou, L.; Liu, X. Efficient degradation of norfloxacin and simultaneous electricity generation in a persulfate-photocatalytic fuel cell system. *Catalysts* **2019**, *9*, 835. [[CrossRef](#)]
34. Rickman, K.A.; Mezyk, S.P. Kinetics and mechanisms of sulfate radical oxidation of β -lactam antibiotics in water. *Chemosphere* **2010**, *81*, 359–365. [[CrossRef](#)] [[PubMed](#)]
35. Olmez-Hanci, T.; Arslan-Alaton, I. Comparison of sulfate and hydroxyl radical based advanced oxidation of phenol. *Chem. Eng. J.* **2013**, *224*, 10–16. [[CrossRef](#)]
36. Zheng, J.; Li, J.; Bai, J.; Xiaohantan, X.; Zeng, Q.; Li, L.; Zhou, B. Efficient degradation of refractory organics using sulfate radicals generated directly from WO₃ photoelectrode and the catalytic reaction of sulfate. *Catalysts* **2017**, *7*, 346. [[CrossRef](#)]
37. Neta, P.; Madhavan, V.; Zemel, H.; Fessenden, R.W. Rate Constants and Mechanism of Reaction of SO₄ with Aromatic Compounds. *J. Am. Chem. Soc.* **1977**, *99*, 163–164. [[CrossRef](#)]
38. Buxton, G.V.; Greenstock, C.L.; Helman, W.P.; Ross, A.B. Critical Review of rate constants for reactions of hydrated electrons, hydrogen atoms and hydroxyl radicals ($\cdot\text{OH}/\text{O}^-$ in Aqueous Solution. *J. Phys. Chem. Ref. Data* **1988**, *17*, 513. [[CrossRef](#)]
39. Tang, W.Z. Huren an Photocatalytic degradation kinetics and mechanism of acid blue 40 by TiO₂/UV in aqueous solution. *Chemosphere* **1995**, *31*, 4171–4183. [[CrossRef](#)]
40. Li, X.; Tang, S.; Yuan, D.; Tang, J.; Zhang, C.; Li, N.; Rao, Y. Improved degradation of anthraquinone dye by electrochemical activation of PDS. *Ecotoxicol. Environ. Saf.* **2019**, *177*, 77–85. [[CrossRef](#)]
41. Waclawek, S.; Lutze, H.V.; Grübel, K.; Padil, V.V.T.; Černík, M.; Dionysiou, D.D. Chemistry of persulfates in water and wastewater treatment: A review. *Chem. Eng. J.* **2017**, *330*, 44–62. [[CrossRef](#)]
42. Yang, J.; Zeng, Z.; Huang, Z.; Cui, Y. Acceleration of persulfate activation by MIL-101(Fe) with vacuum thermal activation: Effect of FeII/FeIII mixed-valence center. *Catalysts* **2019**, *9*, 906. [[CrossRef](#)]

43. Duan, X.; Sun, H.; Kang, J.; Wang, Y.; Indrawirawan, S.; Wang, S. Insights into heterogeneous catalysis of persulfate activation on dimensional-structured nanocarbons. *ACS Catal.* **2015**, *5*, 4629–4636. [[CrossRef](#)]
44. Ji, Y.; Shi, Y.; Yang, Y.; Yang, P.; Wang, L.; Lu, J.; Li, J.; Zhou, L.; Ferronato, C.; Chovelon, J.M. Rethinking sulfate radical-based oxidation of nitrophenols: Formation of toxic polynitrophenols, nitrated biphenyls and diphenyl ethers. *J. Hazard. Mater.* **2019**, *361*, 152–161. [[CrossRef](#)] [[PubMed](#)]
45. Gözmen, B.; Kayan, B.; Gizir, A.M.; Hesenov, A. Oxidative degradations of reactive blue 4 dye by different advanced oxidation methods. *J. Hazard. Mater.* **2009**, *168*, 129–136. [[CrossRef](#)] [[PubMed](#)]
46. Lizama, C.; Freer, J.; Baeza, J.; Mansilla, H.D. Optimized photodegradation of reactive blue 19 on TiO₂ and ZnO suspensions. *Catal. Today* **2002**, *76*, 235–246. [[CrossRef](#)]
47. Tehrani-Bagha, A.R.; Mahmoodi, N.M.; Menger, F.M. Degradation of a persistent organic dye from colored textile wastewater by ozonation. *Desalination* **2010**, *260*, 34–38. [[CrossRef](#)]
48. Bilal, M.; Rasheed, T.; Iqbal, H.M.N.; Li, C.; Wang, H.; Hu, H.; Wang, W.; Zhang, X. Photocatalytic degradation, toxicological assessment and degradation pathway of C.I. Reactive Blue 19 dye. *Chem. Eng. Res. Des.* **2018**, *129*, 384–390. [[CrossRef](#)]
49. Becelic-Tomin, M.; Dalmacija, B.; Rajic, L.; Tomasevic, D.; Kerkez, D.; Watson, M.; Prica, M. Degradation of anthraquinone dye reactive blue 4 in pyrite ash catalyzed fenton reaction. *Sci. World J.* **2014**, *2014*, 234654. [[CrossRef](#)]
50. Lovato, M.E.; Fiasconaro, M.L.; Martín, C.A. Degradation and toxicity depletion of RB19 anthraquinone dye in water by ozone-based technologies. *Water Sci. Technol.* **2017**, *75*, 813–822. [[CrossRef](#)]
51. Radovic, M.; Mitrovic, J.; Kostic, M.; Bojic, D.; Petrovic, M.; Najdanovic, S.; Bojic, A. Comparison of ultraviolet radiation/hydrogen peroxide, Fenton and photo-Fenton processes for the decolorization of reactive dyes. *Hem. Ind.* **2015**, *69*, 657–665. [[CrossRef](#)]
52. Sharma, S.; Patel, S.; Ruparelia, J. Feasibility study on degradation of RR120 dye from water by O₃, O₃/UV and O₃/UV/Persulfate. In *In Multi-Disciplinary Sustainable Engineering: Current and Future Trends, Proceedings of the 5th Nirma University International Conference on Engineering, Ahmedabad, India, 26–28 November 2015*; CRC Press: Boca Raton, FL, USA, 2016; p. 233.
53. Herrmann, H.; Reese, A.; Zellner, R. Time-resolved UV/VIS diode array absorption spectroscopy of SO_x[−] (x=3, 4, 5) radical anions in aqueous solution. *J. Mol. Struct.* **1995**, *348*, 183–186. [[CrossRef](#)]
54. Tan, C.; Gao, N.; Deng, Y.; Zhang, Y.; Sui, M.; Deng, J.; Zhou, S. Degradation of antipyrine by UV, UV/H₂O₂ and UV/PS. *J. Hazard. Mater.* **2013**, *260*, 1008–1016. [[CrossRef](#)] [[PubMed](#)]
55. Shah, N.S.; He, X.; Khan, H.M.; Khan, J.A.; O'Shea, K.E.; Boccelli, D.L.; Dionysiou, D.D. Efficient removal of endosulfan from aqueous solution by UV-C/peroxides: A comparative study. *J. Hazard. Mater.* **2013**, *263*, 584–592. [[CrossRef](#)] [[PubMed](#)]
56. Neta, P.; Huie, R.E.; Ross, A.B. Rate Constants for Reactions of Inorganic Radicals in Aqueous Solution. *J. Phys. Chem. Ref. Data* **1988**, *17*, 1027–1284. [[CrossRef](#)]
57. De Laat, J.; Le, T.G. Kinetics and modeling of the Fe(III)/H₂O₂ system in the presence of sulfate in acidic aqueous solutions. *Environ. Sci. Technol.* **2005**, *39*, 1811–1818. [[CrossRef](#)]
58. Yang, Z.; Su, R.; Luo, S.; Spinney, R.; Cai, M.; Xiao, R.; Wei, Z. Comparison of the reactivity of ibuprofen with sulfate and hydroxyl radicals: An experimental and theoretical study. *Sci. Total Environ.* **2017**, *590*, 751–760. [[CrossRef](#)]
59. Ghauch, A.; Baalbaki, A.; Amasha, M.; El Asmar, R.; Tantawi, O. Contribution of persulfate in UV-254 nm activated systems for complete degradation of chloramphenicol antibiotic in water. *Chem. Eng. J.* **2017**, *317*, 1012–1025. [[CrossRef](#)]
60. Silveira, J.E.; Garcia-Costa, A.L.; Cardoso, T.O.; Zazo, J.A.; Casas, J.A. Indirect decolorization of azo dye Disperse Blue 3 by electro-activated persulfate. *Electrochim. Acta* **2017**, *258*, 927–932. [[CrossRef](#)]
61. Lin, H.; Zhang, H.; Hou, L. Degradation of C. I. Acid Orange 7 in aqueous solution by a novel electro/Fe₃O₄/PDS process. *J. Hazard. Mater.* **2014**, *276*, 182–191. [[CrossRef](#)]
62. Liang, C.; Wang, Z.S.; Bruell, C.J. Influence of pH on persulfate oxidation of TCE at ambient temperatures. *Chemosphere* **2007**, *66*, 106–113. [[CrossRef](#)]
63. Asghar, A.; Bello, M.M.; Raman, A.A.A.; Daud, W.M.A.W.; Ramalingam, A.; Zain, S.B.M. Predicting the degradation potential of Acid blue 113 by different oxidants using quantum chemical analysis. *Heliyon* **2019**, *5*, e02396. [[CrossRef](#)]

64. Lang, A.R. *Dyes and Pigments: New Research*; Nova Science Publishers: Hauppauge, NY, USA, 2009; ISBN 978-1-60876-195-1.
65. Cinar, Z. The Role of Molecular Modeling in TiO₂ Photocatalysis. *Molecules* **2017**, *22*, 556. [\[CrossRef\]](#)
66. Liu, S.; Rong, C.; Lu, T. Information conservation principle determines electrophilicity, nucleophilicity, and regioselectivity. *J. Phys. Chem. A* **2014**, *118*, 3698–3704. [\[CrossRef\]](#) [\[PubMed\]](#)
67. Xiao, R.; Ye, T.; Wei, Z.; Luo, S.; Yang, Z.; Spinney, R. Quantitative Structure–Activity Relationship (QSAR) for the Oxidation of Trace Organic Contaminants by Sulfate Radical. *Environ. Sci. Technol.* **2015**, *49*, 13394–13402. [\[CrossRef\]](#) [\[PubMed\]](#)
68. Ziegler, P.; Sree, K.S.; Appenroth, K.J. Duckweeds for water remediation and toxicity testing. *Toxicol. Environ. Chem.* **2016**, *98*, 1127–1154. [\[CrossRef\]](#)
69. Žaltauskaitė, J.; Sujetovienė, G.; Čypaitė, A.; Aužbikavičiūtė, A. Lemna Minor as a Tool for Wastewater Toxicity Assessment and Pollutants Removal Agent. In Proceedings of the 9th International Conference on Environmental Engineering, Vilnius, Lithuania, 22–23 May 2014.
70. Mkandawire, M.; Teixeira Da Silva, J.A.; Dudel, E.G. The lemna bioassay: Contemporary issues as the most standardized plant bioassay for aquatic ecotoxicology. *Crit. Rev. Environ. Sci. Technol.* **2014**, *44*, 154–197. [\[CrossRef\]](#)
71. Sackey, L.N.A.; Kočí, V.; van Gestel, C.A.M. Ecotoxicological effects on Lemna minor and Daphnia magna of leachates from differently aged landfills of Ghana. *Sci. Total Environ.* **2020**, *698*, 134295. [\[CrossRef\]](#)
72. Castro, A.M.; Nogueira, V.; Lopes, I.; Rocha-Santos, T.; Pereira, R. Evaluation of the potential toxicity of effluents from the textile industry before and after treatment. *Appl. Sci.* **2019**, *9*, 3804. [\[CrossRef\]](#)
73. Kudlek, E. Identification of Degradation By-Products of Selected Pesticides during Oxidation and Chlorination Processes. *Ecol. Chem. Eng. S* **2019**, *26*, 571–581. [\[CrossRef\]](#)
74. Neamtu, M.; Siminiceanu, I.; Yediler, A.; Kettrup, A. Kinetics of decolorization and mineralization of reactive azo dyes in aqueous solution by the UV/H₂O₂ oxidation. *Dye. Pigment.* **2002**, *53*, 93–99. [\[CrossRef\]](#)
75. Palencia, M.; Martínez, J.M.; Arrieta, Á. Removal of Acid Blue 129 dye by Polymer-Enhanced Ultrafiltration (PEUF). *J. Sci. Technol. Appl.* **2017**, *2*, 65–74. [\[CrossRef\]](#)
76. Stumm, W.; Morgan, J.J. *Aquatic Chemistry: Chemical Equilibria and Rates in Natural Waters*, 3rd ed.; Wiley: Hoboken, NJ, USA, 2012; ISBN 1118591488.
77. Silvestri, D.; Wacławek, S.; Venkateshaiah, A.; Krawczyk, K.; Sobel, B.; Padil, V.V.T.; Černík, M.; Varma, R.S. Synthesis of Ag nanoparticles by a chitosan-poly(3-hydroxybutyrate) polymer conjugate and their superb catalytic activity. *Carbohydr. Polym.* **2020**, *232*, 115806. [\[CrossRef\]](#)
78. Hanwell, M.D.; Curtis, D.E.; Lonie, D.C.; Vandermeersch, T.; Zurek, E.; Hutchison, G.R. Avogadro: An advanced semantic chemical editor, visualization, and analysis platform. *J. Cheminform.* **2012**, *4*, 17. [\[CrossRef\]](#)
79. Neese, F. The ORCA program system. *WIREs Comput. Mol. Sci.* **2012**, *2*, 73–78. [\[CrossRef\]](#)
80. Lu, T.; Chen, F. Multiwfn: A multifunctional wavefunction analyzer. *J. Comput. Chem.* **2012**, *33*, 580–592. [\[CrossRef\]](#)
81. Fu, R.; Lu, T.; Chen, F.W. Comparing methods for predicting the reactive site of electrophilic substitution. *Acta Phys.-Chim. Sin.* **2014**, *30*, 628–639.
82. Santana, C.M.; Ferrera, Z.S.; Padrón, M.E.T.; Rodríguez, J.J.S. Methodologies for the extraction of phenolic compounds from environmental samples: New approaches. *Molecules* **2009**, *14*, 298–320. [\[CrossRef\]](#) [\[PubMed\]](#)

